MDPI

Article

Drive Bunch Train for the Dielectric Trojan Horse Experiment at the Argonne Wakefield Accelerator

Gerard Andonian [1,2,*], Nathan Burger [2], Nathan Cook [3], Scott Doran [4], Tara Hodgetts [2], Seongyeol Kim [4], Gwanghui Ha [4,5], Wanming Liu [4], Walter Lynn [1], Nathan Majernik [1], John Power [3], Alexey Pronikov [2], James Rosenzweig [1] and Eric Wisniewski [4]

1   Department of Physics and Astronomy, University of California Los Angeles , Los Angeles, CA 90095, USA
2   RadiaBeam Technologies, Santa Monica, CA 90404, USA
3   RadiaSoft LLC., Boulder, CO 80301, USA
4   Argonne Wakefield Accelerator, Argonne National Laboratory, Lemont, IL 60439, USA
5   Department of Physics, Northern Illinois University, DeKalb, IL 60115, USA
*   Correspondence: gerard@physics.ucla.edu

Abstract: The recently demonstrated concept of the plasma photocathode, whereby a high-brightness bunch is initialized by laser ionization within a plasma wakefield acceleration bubble, is informally referred to as Trojan Horse wakefield acceleration. In a similar vein, the dielectric Trojan Horse concept incorporates a dielectric-lined waveguide to support a charged particle beam-driven accelerating mode and uses laser initiated ionization of neutral gas within the waveguide to generate a witness beam. One of the advantages of the dielectric Trojan Horse concept is the reduced requirements in terms of timing precision due to operation at a lower frequency. In this paper, we present experimental results on the generation and characterization of a four-bunch drive train for resonant excitation of wakefields in a cylindrical dielectric waveguide conducted at the Argonne Wakefield Accelerator facility. The results lay the foundation for the demonstration of a plasma photocathode scheme within a dielectric wakefield accelerating structure. Modifications to improve capture efficiency with improved beam transmission are suggested as well.

Keywords: dielectric wakefield acceleration; plasma photocathode

1. Introduction

Advanced particle acceleration techniques that harness wakefield excitation within a medium have demonstrated the capacity to attain accelerating gradients orders of magnitude greater than traditional methods. Further innovative concepts are integral to advancing the delivery of high beam quality for next-generation applications using advanced acceleration technology. In the plasma photocathode concept, neutral gas particles are ionized using a high intensity laser within a beam-driven plasma wakefield bubble. The plasma photocathode has the potential to achieve near nanometer scale emittance and low energy spread [1]. Recently, an experimental program at the SLAC FACET facility demonstrated the core principles of the plasma photocathode [2], informally referred to as "Trojan Horse" acceleration. The Trojan Horse method requires a dual-gaseous mixture of low and high ionization threshold gases for wakefield production and witness beam generation, respectively. It has strict timing demands, on the scale of 10s of femtoseconds, which requires precise methods of temporal characterization [3–6]. A modified version of the Trojan Horse concept, referred to as "dielectric Trojan Horse", incorporates a beam-driven dielectric wakefield accelerator (DWA) [7,8] in place of the plasma accelerator. The DWA, which consists of a dielectric lined waveguide, is filled with a gas that is then ionized by an intense laser pulse, in a similar vein to the plasma-based Trojan Horse. Although the gradients in the DWA are not as intense as in the plasma case, $\sim$GV/m fields have been

achieved [9]. However, the longer wavelength scales in the DWA system allow for more relaxed requirements in terms of drive beam properties and laser timing.

The plasma photocathode in a DWA (Figure 1), or dielectric Trojan Horse, has been conceptualized for an experiment at the Argonne Wakefield Accelerator (AWA) facility. A drive train of four bunches, with spacing equal to the fundamental wavelength of the structure, is generated to resonantly excite the accelerating mode [10]. A bunch train, rather than a single high-charge bunch [11], is considered in order to keep the beam emittance at a manageable level for optimal transport through the DWA. As the wakefield is excited inside the gas-filled channel, a laser pulse is injected at an appropriate phase behind the last bunch. The laser pulse ionizes the gas, liberating electrons that are then captured by the wakefield and accelerated through the structure. The newly formed witness beam can have a small emittance and be accelerated to high energy through the structure.
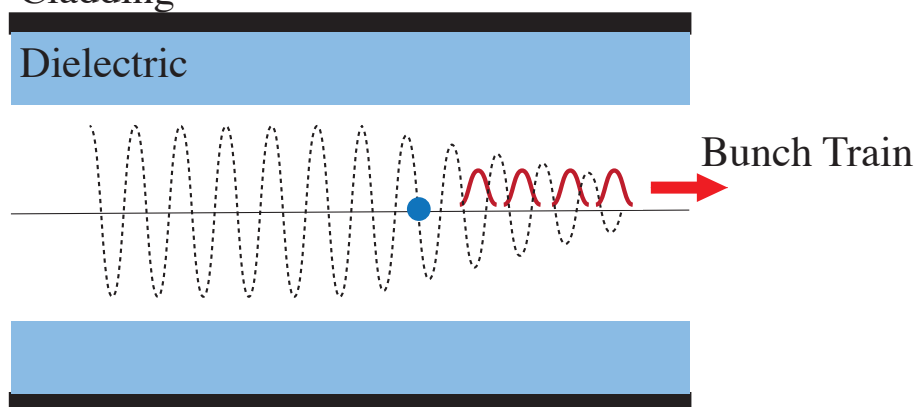

Figure 1. Illustrative sketch of the dielectric Trojan Horse concept. The driver is a four-bunch train (red) that travels down the axis of a gas-filled dielectric-lined waveguide with metallic cladding. A wakefield is supported within the channel (dotted line). A laser is injected (blue dot) at an appropriate phase of the wakefield to ionize the gas and liberate electrons. The newly liberated electrons are captured and accelerated, comprising the witness beam.

The practical individual subcomponents of the dielectric Trojan Horse system, including the fabrication of the DWA with gas delivery and subsequent development of laser injection with appropriate timing, have previously been demonstrated at the AWA and reported elsewhere [12]. The work presented in this paper focuses on the generation and preparation of a four-bunch drive train at the AWA, which is a critical component that dictates the wakefield strength and modal purity of the dielectric Trojan Horse scheme. The longitudinal phase space was recorded for cases of the drive train without the structure to ensure proper temporal spacing, then again while going through the structure to evaluate wakefield effects, manifested as energy modulation of the drive bunches. The results show that full charge transmission was a challenge at moderate beam energy; however, the partial transmitted charge shows wakefield strengths that are comparable to analytic results. With appropriate improvements in beam emittance and energy, wakefield amplitudes scaled to higher charge transmission would allow the witness beam to be captured and accelerated. Suggestions on using advanced DWA structure geometries such as tapered waveguides are presented as well.

2. Materials and Methods

The dielectric Trojan Horse experiment is hosted at the Argonne Wakefield Accelerator (AWA). The AWA photo-injector and linac sections generate and accelerate an electron beam to 60 MeV. For the dielectric Trojan Horse experiments, the drive beam is a four-bunch train with variable spacing. The intra-bunch spacing is controlled by manipulating laser pulses, using multiple beamsplitters on different delay arms that are then recombined to illuminate

the cathode. The charge is constrained between 4–5 nC per bunch to provide reduced beam emittance for beam transmission at the AWA. In addition, excessive charge that generates fields above ∼few GV/m may illicit breakdown and damping of the wakefield, which has been observed at very high fields in prior experiments [13].

The bunch train is transported and focused into an interaction chamber using quadrupole magnets in triplet configuration (see Figure 2). The quadrupole lattice focuses the bunches to a ∼40 µm spot size at the longitudinal location of the DWA center. The interaction chamber houses the dielectric structure on a movable stage. The beamline incorporates YAG profile screens with Basler CCD cameras that are used for beam transverse size and centroid measurements. Screens are located equidistant before and after the interaction chamber, and the centroid measurements at these screens are used to define the central axis onto which the DWA axis is aligned. Inside the interaction chamber, the longitudinal location of the DWA structure includes a secondary mount co-located with the center of the structure, with an additional YAG profile screen. The central screen measurement allows for accurate determination of the beam spot size for optimum transport through the structure. Further downstream are two additional screens that are used in conjunction with other screens for beam emittance measurements. Finally, the beamline terminates in a diagnostic station that includes a transverse deflecting cavity for temporal measurements and a dipole magnet spectrometer for energy measurements. The intra-bunch spacing during beam preparation, without the structure inserted, is monitored and adjusted based on the profiles from the transverse deflecting cavity. When used in tandem, the deflecting cavity and dipole spectrometer enable measurement of the complete longitudinal phase space (LPS).
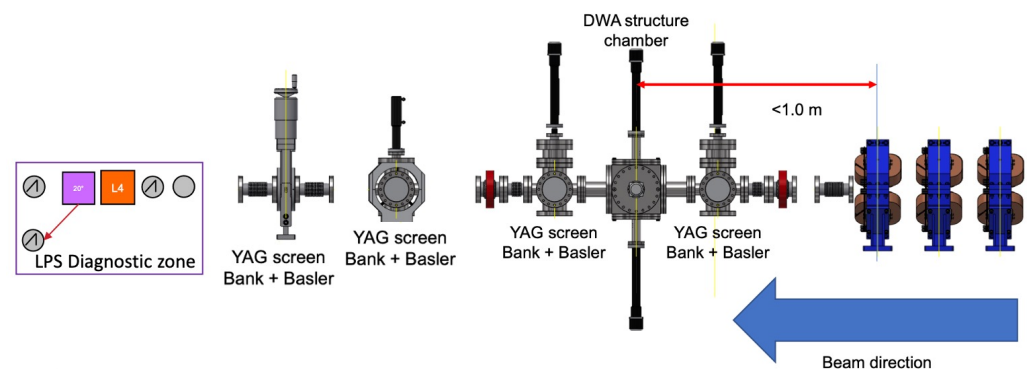

Figure 2. Experiment sketch of the beamline at AWA. The beam direction is right to left. The 60 MeV drive train is focused down into the DWA structure chamber by a triplet configuration of quadrupole magnets. YAG screens provide measurements of the beam size and centroid position. A diagnostic zone allows for measurements of the full longitudinal phase space.

The DWA is a cylindrical dielectric-lined waveguide comprised of SiO_2 (ϵ = 3.85) with a thickness of 500 µm and a thin copper cladding. The inner channel which the bunches pass through has a diameter of 500 µm [12]. The wavelength of the fundamental mode excited in the dielectric with these parameters is 2.99 mm. The dielectric waveguide incorporates a small hole (<400 µm diameter), into which a capillary insert with a nozzle is fitted. The hole is drilled through one side of the cladding and dielectric, and the nozzle insert allows for the flow of xenon gas into the dielectric structure. Xenon is chosen because the gas is inert, has a negligible effect on the quantum efficiency of the cathode in case of contamination, and has an ionization threshold that is attainable with the AWA injection laser. The gas delivery nozzle has an inconsequential effect on the generation of the wakefield, as the wakefield wavelength (∼3 mm) is much greater than the nozzle insert diameter. The relevant beam and structure parameters are summarized in Table 1.

Table 1. Parameter list for the bunch drive train and dielectric-lined waveguide.

Parameter	Value
Electron Bunch	
Beam Energy (U_{beam})	59.5 MeV
Bunch Charge (Q)	4 nC
Bunch Duration (σ_t)	3 ps
Normalized Emittance (ϵ_n)	39 mm mrad (single bunch)
Spot Size at DWA (σ_r)	40 μm
Number of Bunches (N)	4
Bunch Spacing (Δz)	3 mm
Projected Emittance	67 mm mrad (all bunches)
Dielectric Waveguide	
Inner Diameter (a)	500 μm
Outer Diameter (b)	1500 μm
Relative Permittivity (ϵ)	3.85
Length (L)	2 cm

3. Results

The preparation of the bunch train at the AWA was focused on generating bunchlets with near-homogenous qualities and variable spacing. To mitigate collective effects from the transport line, the mean charge, mean energy, and energy spread of each bunch should be similar. In the initial measurements, charge balance was accomplished at the photocathode by having four individual laser relay lines to generate each of the bunches in the train. With the appropriate position of polarizing beamsplitters and some iterative steps to measure the charge of each individual bunch with a downstream Faraday cup, a mean charge of 4 nC per bunch was achieved. Second, in order to ensure the same central energy and energy spread of each bunch, the laser injection had to occur at the appropriate phase in the accelerating bucket cycle. With appropriate phasing of the photogun and linac sections, the bunch energy distribution was measured on the dipole spectrometer on an individual basis. The spectrometer located at the end of the beamline indicated a mean central energy of 59.5 MeV with an energy spread of ∼2% per bunch. The AWA RF gun and six linac cavity phases (L-band, 1.3 GHz structures) are adjusted to generate a bunch train with near-identical fractional energy spread. The RF gun phase was adjusted to +40° from zero-phase, −18° from on-crest for the first two linac sections, and −21° from on-crest for the next four linac sections. This configuration avoids large beam mismatches due to chromatic aberration among the bunches during the final beam focusing before entering the dielectric tube.

With the energy and charge dialed in for each bunch in the drive train, the bunch spacing between each bunchlet was then homogenized to the nominal value of 3 mm. The spacing was accomplished using the individual laser relay lines and changing the delay of the laser arrival at the cathode while monitoring the screen from the transverse deflecting cavity. After numerous iterations, 3 mm bunch spacing with equal charge and energy was achieved (Figure 3a). The obtained results compare very well with simulations of the AWA beamline to generate the bunch train using OPAL [14] (shown in Figure 3b).

After the energy, energy spread, and bunch spacing are established, the transverse emittance is optimized. The emittance is measured using a slit-scan method [15]. In this procedure, a single bunch is first transported through the beam line with a nominal charge of 4 nC. The emittance of this single bunch is minimized by varying the solenoid current value at the RF gun. In this case, an emittance value of 39 mm-mrad was recorded for the single bunch. The other three bunches are then added and the projected emittance of the bunch train is measured. The minimum calculated beta functions were approximately 4 cm in the horizontal direction and 3 cm in the vertical; this is discussed further in the next section. For the bunch train, a projected emittance of 67 mm-mrad was recorded at a total charge of 16 nC, or 4 nC per bunch.
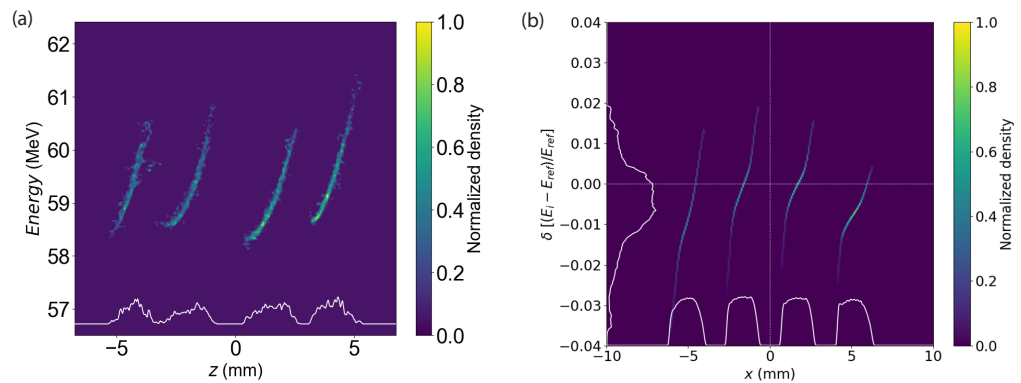
Figure 3. (**a**) Measured longitudinal phase space at the end of the beamline, showing the nearly equal charge and energy of the bunchlets with appropriate spacing. (**b**) OPAL simulations of the bunch train generation used to design the beamline transport.

　　　With the drive train prepared, the next important measurement is the transmission of the train through the dielectric structure. Using the settings for a bunch focused down to a 40 μm transverse spot size at the location of the structure center, all four bunches' centroid positions are marked on the profile screens. The dielectric structure is then positioned to the pre-aligned beam trajectory marks. The beam is adjusted by fine-tuning both the upstream steering magnets and the quadrupole magnets, which may contribute to transverse motion if the bunches are not exactly centered. The relative transmission of the four-bunch train is plotted in Figure 4 for 400 consecutive shots after the tuning process. For this set of data, the mean transmission was 38.5% (6.2 nC), while shots as high as 47% (7.5 nC) were recorded. The relative transmission quoted here is based on a total charge of 16 nC in the drive train. Individual shots were time-tagged and correlated to longitudinal phase space measurements during post-analysis.
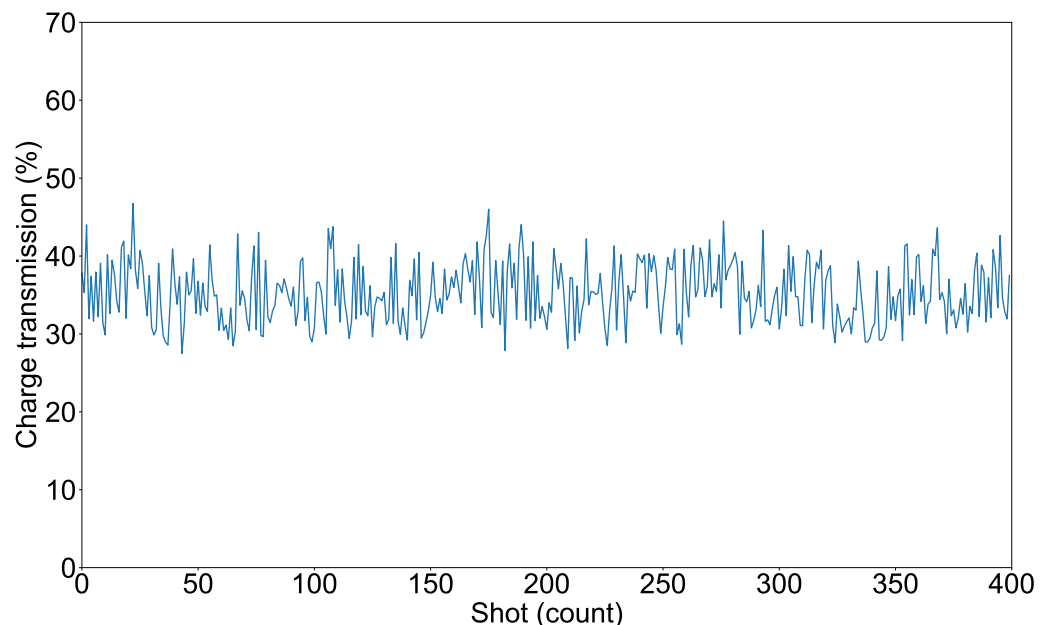

Figure 4. Relative transmission of four-bunch train through dielectric structure for 400 consecutive shots. Mean value is 38.5%, and shots as high as 47% were observed.

　　　As transmission is maximized through the structure, the longitudinal phase space of the bunch train is recorded at the diagnostic station. Figure 5a shows a raw sample shot of the phase space. From the image, the four bunches spaced in time are evident; however,

additional modulation and alteration of the bunches in terms of their energy can be seen as well. This is reflective of the bunch train's interaction with the self-wakefield it is generating, with the highest change in energy being evident in the final bunches. Because the first bunch initiates the wakefield, it is the least affected by the fields. The energy modulation of the bunches is consistent with the expected wavelength of the fundamental mode, as each bunch is sampling the decelerating component of the sinusoidal field, which is another verification that the bunch spacing is nearly optimal for the field to extract energy from the beam. In addition, based on the energy change of the last bunchlet, the field amplitude observed over the 20 mm structure can be estimated as slightly greater than ~200 MeV/m. This figure is consistent with the estimates of 38.5%, or 6.2 nC, for the charge transmission through the structure.
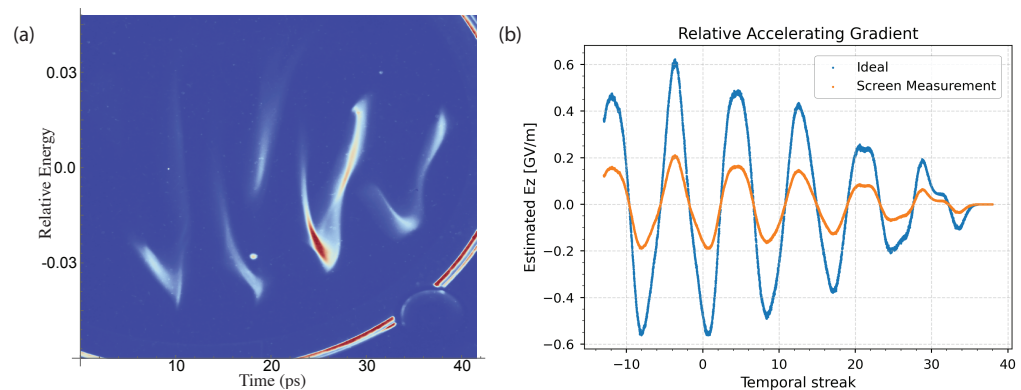

Figure 5. (**a**) Raw screen image of the full longitudinal phase space of the four bunch train after interaction in the dielectric structure. The energy modulation corresponding to the time scale of the fundamental mode can be observed. The bright red partial circle is light reflecting from the screen mount. (**b**) Estimated fields for the measured bunch train calculated by fitting the scaled fields from simulations to the screen measurements, showing ideal fields generated with total charge of 14 nC, or 87.5% transmission, corresponding to an expected upgrade in beam transmission.

4. Discussion

The main reasons that full transmission is not achieved, as shown in Figure 4, are the different focusing levels for the bunches at various RF phases at injection and the effects of transverse wakefields. The bunches may have differing charges after traversing the dielectric structure due to the different initial Twiss parameters of each bunch. Because each bunch experiences a different RF phase due to the finite time separation, a distinct RF focusing is applied to each, leading to different initial beta functions. Figure 6b shows an OPAL simulation of the horizontal phase space at the waist position in the center of the structure. Each bunch has a disparate horizontal phase space; if the Twiss parameters were the same, then the horizontal phase space would look like a single ellipse instead of four distinct branches. Therefore, in the current experimental setting we expect some of the bunches to be focused more than others, as can be seen in Figure 6a, where we see the defocusing effect on the third and fourth bunches.

The divergent bunches lead to another reason for non-optimal transmission through the dielectric structure due to the effects of transverse wakefields [16]. Transverse wakefields are generated by the front of the bunch train, and affect the rear of the train due to quadrupole-like focusing/defocusing. The effect is exacerbated due to off-axis particle transmission, consequently leading to emittance growth and subsequent partial beam breakup via the growth of transverse instability.
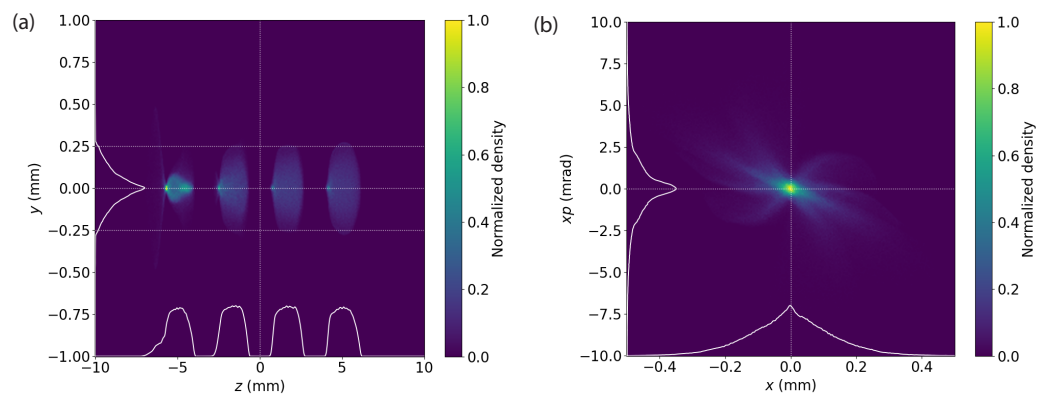
Figure 6. (**a**) OPAL simulation of transverse-to-longitudinal correlation (y–z) of four-bunch train at the waist position. The dashed line shows the 0.5 mm inner diameter of the structure. (**b**) Horizontal phase space at the waist position for the four bunches.

The transmission of the bunch train through the structure is critical for high-amplitude wakefields. The field amplitude is directly proportional to the charge; as shown in the experimental results, the charge in the last two bunchlets begins to deteriorate. Achieving maximal field is critical in the dielectric Trojan Horse scenario, as unlike other two-beam wakefield acceleration methods, the freshly ionized electrons start at rest and must be captured by the field [17]. As the bunch emittance grows along the train, the individual bunchlet charge decreases, and the overall contribution to the wakefield decreases as well. Figure 5b shows a comparison of the measured wakefields from the longitudinal phase space diagnostic screen and the simulated results for an ideal transmission situation. The estimated longitudinal field as a function of longitudinal coordinate is attained from the beam modulation projections of the screen data, then scaled to the relative energy change of the particles. From this measurement, the estimated peak field after the bunch train is 210 MV/m. The ideal transmission case is shown for comparison. For the purposes of this simulation, ideal transmission refers to 14 nC transmission, and the peak field exceeds 600 MV/m. The expected peak field for ideal transmission is important in the context of the dielectric Trojan Horse plasma photocathode experiment because the calculated trapping threshold for using the structure parameters is about 500 MV/m. The comparison shows that improving charge transmission is of paramount importance.

In order to maximize charge transmission and the resulting accelerating gradient, a number of improvements can be considered. First, the AWA facility will undergo a photoinjector upgrade to allow for higher energy beams and improved emittance with the introduction of an axisymmetric photoinjector [18]. The injector used for the present study includes side-coupling RF ports that affect the field quality during acceleration, which in turn affects the minimum attainable emittance. Corrective measures are applied to optimize the downstream beam quality. The introduction of symmetrized RF fields will allow for similar charge beams with reduced emittance compared to the current study without the need for excessive corrections, which may have adverse beam effects. This reduced emittance will lead to smaller spot sizes and greater charge transmission through the structure. In addition, another benefit of smaller beam spot sizes is that different geometry structures, especially structures with smaller diameter, can be employed to achieve even greater field gradients.

Second, the expected transmission through the 2 cm dielectric can be immediately improved with experimental setup modifications. The Twiss parameters from OPAL simulations when using the simulated beam are shown in Figure 7. Here, the 2 cm dielectric tube is placed 26.95 m from the photoinjector cathode surface; the minimum beta function achieved in the horizontal and vertical planes is approximately 4 cm and 3 cm, respectively. Space charge effects are included in the simulations. The waist position is 0.43 m away from the edge of the last quadrupole magnet in the final focusing triplet. When compared to the

currently reported experimental setup, with an average of 6.2 nC transmitted, the distance between the dielectric tube and the last quadrupole magnet is ~1.0 m due to beamline constraints. The charge transmission can be directly improved to 12 nC by placing the waist position closer to the last quadrupole magnet optimized to the correct focal position, albeit in a slightly modified experimental layout. For even greater charge transmission, solutions using strong gradient permanent magnet quadrupoles [19] are possible and would allow the use of higher charge bunches.

Figure 7. OPAL-simulated RMS beam size and beta functions around the waist position. Note that the RMS quantities of all the bunches (projected) are shown. The green shaded area indicates a dielectric tube region 2 cm in length.

The timing and spacing between bunches is another significant consideration, as the appropriate spacing generates a homogeneous mode due to resonant excitation. Simulations were performed in order to understand the consequences of the bunch spacing as it pertains to acceleration strength in the structure. As shown in the simulation of Figure 8a, when the 3 mm spacing is dialed in to match the fundamental mode, there is no contribution to higher-order modes. However, in the case of a non-optimized 3.34 mm spacing, there is an excitation of a second mode, which is not used for acceleration. Figure 8b shows the calculated longitudinal field for different spacings. An enhancement in the amplitude to 600 MV/m is observed for the ideal spacing case compared to the non-ideal case. These results stress the importance of controlling the bunch train parameters with spacing equal to the fundamental wavelength in the structure. For the purposes of the wakefield strengths shown in Figure 8, the charge transmission propagating through the dielectric cylinder corresponds to 14 nC, which is consistent with the peak value for the estimated beam phase space distribution.

For plasma photocathode applications, advanced dielectric structures with tapers have been designed with the goal of enhancing the trapping condition. By varying the thickness of the dielectric along the axis, the operating wavelength is changed and the capture threshold can be modified. The tapered structure offers a compromise between operating at slightly lower frequencies and achieving higher longitudinal gradients. Figure 9 shows a CST simulation of a suggested tapered geometry and the associated electric fields. For this case, the tapered structure has an inner diameter of 0.2 mm and an outer diameter that varies from 0.65 mm to 0.75 mm. The charge transmitted through the structure is 14 nC. The resulting fields for the tapered structure exceed the trapping threshold, and

offer a promising path forward for enhanced capture and acceleration with the nascent AWA beamline upgrade.
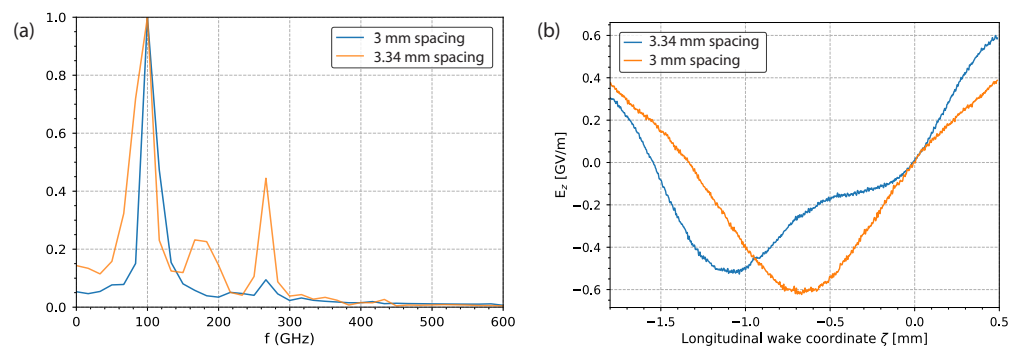

Figure 8. (**a**) Simulation of the spectral content of the accelerating mode for bunch trains with 3.34 mm and 3 mm spacing. (**b**) Local electric field at the first accelerating region for bunch trains with 3.34 mm and 3 mm spacing in a cylindrical structure.
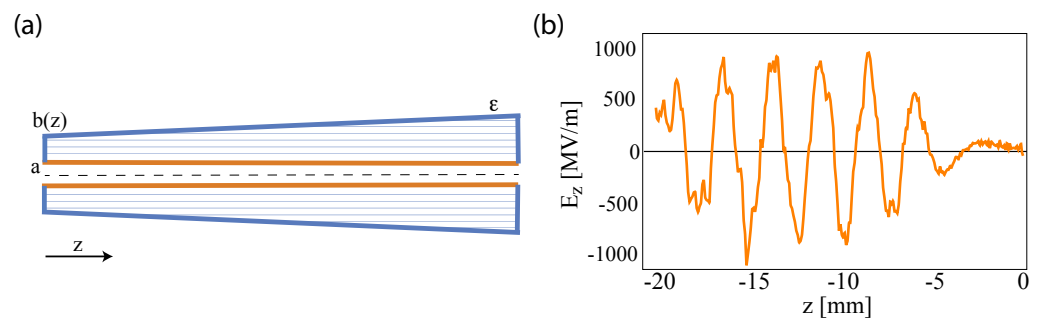

Figure 9. (**a**) Sketch of the tapered DWA structure with inner radius a and outer radius b(z), now a function of the longitudinal coordinate (also corresponding to thickness of the dielectric with permittivity ϵ). (**b**) Calculation of the electric field excitation, reaching 950 MV/m for the tapered structure with a = 0.2 mm and b varying from $0.65 - 0.75$ mm over a length of 2 cm.

5. Conclusions

Studies were undertaken to prepare and evaluate a four-bunch drive train for an upcoming experiment that will incorporate a plasma photocathode. The design parameters were achieved, except for the longitudinal field amplitude, which was lower than the trapping amplitude. The four-bunch drive train was generated at 60 MeV with equal charge (4 nC) and intrabunch spacing of 3 mm for optimal resonant excitation of the fundamental mode in the DWA structure. The observed modulation of the bunch as it traversed the DWA showed behavior consistent with energy transfer to the wakefield; a longitudinal electric field of 210 MeV/m was estimated at a reduced charge transmission, which is consistent with simulation results. For the plasma photocathode experiments using the high-frequency dielectric structure as described above, the field generated from limited charge transmission is below the capture threshold. However there is a clear pathway to enhancing the longitudinal fields in upcoming studies. The enhancements include improved beam emittance from a nascent AWA photoinjector upgrade that will allow a smaller spot and higher transmission to be reached through the dielectric structure. In addition, a modified experimental chamber would allow the DWA structure to be placed closer to the optimal focal point, and studies on optimization to account for bunch-to-bunch RF focusing could improve overall transmission. It is important to note that other methods of achieving small spots over the length of the dielectric capillary traversal are available, such as the addition of in-vacuum permanent magnet quadrupole magnets, which can have very high magnetic field gradients and lead to high charge transmission. When the maximum achievable field is attained without breakdown, other advanced structures, such as a tapered

DWA, can be tested to optimize the capture and acceleration of the witness beam. The reported results demonstrate that the quality of the drive beam is critical for plasma photocathode studies in advanced accelerators.

References

1. Hidding, B.; Pretzler, G.; Rosenzweig, J.; Königstein, T.; Schiller, D.; Bruhwiler, D. Ultracold Electron Bunch Generation via Plasma Photocathode Emission and Acceleration in a Beam-Driven Plasma Blowout. *Phys. Rev. Lett.* **2012**, *108*, 035001. [CrossRef]
2. Deng, A.; Karger, O.S.; Heinemann, T.; Knetsch, A.; Scherkl, P.; Manahan, G.G.; Beaton, A.; Ullmann, D.; Wittig, G.; Habib, A.F.; et al. Generation and acceleration of electron bunches from a plasma photocathode. *Nat. Phys.* **2019**, *15*, 1156. [CrossRef]
3. Hunt-Stone, K.; Ariniello, R.; Doss, C.; Lee, V.; Litos, M. Electro-optic sampling beam position monitor for relativistic electron beams. *Nucl. Instrum. Methods Phys. Res. Sect. A Accel. Spectrom. Detect. Assoc. Equip.* **2021**, *999*, 165210. [CrossRef]
4. Scherkl, P.; Knetsch, A.; Heinemann, T.; Sutherland, A.; Habib, A.F.; Karger, O.S.; Ullmann, D.; Beaton, A.; Manahan, G.G.; Xi, Y.; et al. Plasma photonic spatiotemporal synchronization of relativistic electron and laser beams. *Phys. Rev. Accel. Beams* **2022**, *25*, 052803. [CrossRef]
5. Hidding, B.; Assmann, R.; Bussmann, M.; Campbell, D.; Chang, Y.Y.; Corde, S.; Cabadağ, J.C.; Debus, A.; Döpp, A.; Gilljohann, M.; et al. Progress in Hybrid Plasma Wakefield Acceleration. *Photonics* **2023**, *10*, 99. [CrossRef]
6. Marchetti, B.; Grudiev, A.; Craievich, P.; Assmann, R.; Braun, H.H.; Catalan Lasheras, N.; Christie, F.; D'Arcy, R.; Fortunati, R.; Ganter, R.; et al. Experimental demonstration of novel beam characterization using a polarizable X-band transverse deflection structure. *Sci. Rep.* **2021**, *11*, 3560. [CrossRef]
7. Pacey, T.; Saveliev, Y.; Xia, G.; Smith, J. Simulation studies for dielectric wakefield programme at CLARA facility. *Nucl. Instrum. Methods Phys. Res. Sect. A Accel. Spectrom. Detect. Assoc. Equip.* **2018**, *909*, 261–265. [CrossRef]
8. Nie, Y.; Assmann, R.; Dorda, U.; Marchetti, B.; Weikum, M.; Zhu, J.; Hüning, M. Potential applications of the dielectric wakefield accelerators in the SINBAD facility at DESY. *Nucl. Instrum. Methods Phys. Res. Sect. A Accel. Spectrom. Detect. Assoc. Equip.* **2016**, *829*, 183–186. [CrossRef]
9. O'Shea, B.D.; Andonian, G.; Barber, S.K.; Fitzmorris, K.L.; Hakimi, S.; Harrison, J.; Hoang, P.D.; Hogan, M.J.; Naranjo, B.; Williams, O.B.; et al. Observation of acceleration and deceleration in gigaelectron-volt-per-metre gradient dielectric wakefield accelerators. *Nat. Commun.* **2016**, *7*, 12763. [CrossRef]
10. Andonian, G.; Williams, O.; Wei, X.; Niknejadi, P.; Hemsing, E.; Rosenzweig, J.B.; Muggli, P.; Babzien, M.; Fedurin, M.; Kusche, K.; et al. Resonant excitation of coherent Cerenkov radiation in dielectric lined waveguides. *Appl. Phys. Lett.* **2011**, *98*, 202901. [CrossRef]
11. Tsakanov, V.M. On collinear wake field acceleration with high transformer ratio. *Nucl. Instrum. Methods Phys. Res. Sect. A Accel. Spectrom. Detect. Assoc. Equip.* **1999**, *432*, 202–213. [CrossRef]
12. Andonian, G.; Campese, T.; Cook, M.; Lynn, W.; Majernik, N.; Rosenzeig, J.; Yu, V.; Doran, S.; Ha, G.; Power, J.; et al. Dielectric Wakefield Acceleration With A Laser Injected Witness Beam. In Proceedings of the 12th International Particle Accelerator Conference, Campinas, Brazil, 24–28 May 2021; Volume A15, p. 481.
13. O'Shea, B.D.; Andonian, G.; Barber, S.K.; Clarke, C.I.; Hoang, P.D.; Hogan, M.J.; Naranjo, B.; Williams, O.B.; Yakimenko, V.; Rosenzweig, J.B. Conductivity Induced by High-Field Terahertz Waves in Dielectric Material. *Phys. Rev. Lett.* **2019**, *123*, 134801. [CrossRef]
14. Adelmann, A.; Arbenz, P.; Ineichen, Y. A fast parallel Poisson solver on irregular domains applied to beam dynamics simulations. *J. Comput. Phys.* **2010**, *229*, 4554–4566. [CrossRef]

15. Catani, L.; Chiadroni, E.; Cianchi, A.; Tazzari, S.; Boscolo, M.; Castellano, M.; Di Pirro, G.; Ferrario, M.; Fusco, V.; Filippetto, D.; et al. Design and characterization of a movable emittance meter for low-energy electron beams. *Rev. Sci. Instrum.* **2006**, *77*, 093301. [CrossRef]

16. Li, C.; Gai, W.; Jing, C.; Power, J.G.; Tang, C.X.; Zholents, A. High gradient limits due to single bunch beam breakup in a collinear dielectric wakefield accelerator. *Phys. Rev. Spec. Top. Accel. Beams* **2014**, *17*, 091302. [CrossRef]

17. Manahan, G.G.; Deng, A.; Karger, O.; Xi, Y.; Knetsch, A.; Litos, M.; Wittig, G.; Heinemann, T.; Smith, J.; Sheng, Z.M.; et al. Hot spots and dark current in advanced plasma wakefield accelerators. *Phys. Rev. Accel. Beams* **2016**, *19*, 011303. [CrossRef]

18. Frame, E.; Marzouk, A.A.; Chubenko, O.; Doran, S.; Piot, P.; Power, J.; Wisniewski, E. Opportunities for Bright-Beam Generation at the Argonne Wakefield Accelerator (AWA). *Instruments* **2023**, *7*, 48. [CrossRef]

19. Li, R.K.; Musumeci, P. Single-Shot MeV Transmission Electron Microscopy with Picosecond Temporal Resolution. *Phys. Rev. Appl.* **2014**, *2*, 024003. [CrossRef]